The Astrophysical Journal Letters, 941:L33 (10pp), 2022 December 20 https://doi.org/10.3847/2041-8213/aca806

White Dwarf—Red Giant Star Binaries as Type Ia Supernova Progenitors: With and without Magnetic Confinement

Iminhaji Ablimit[1,2], Philipp Podsiadlowski[3], Rosanne Di Stefano[4], Saul A. Rappaport[5], and James Wicker[6]
[1] CAS Key Laboratory for Optical Astronomy, National Astronomical Observatories, Chinese Academy of Sciences, Beijing 100012, People's Republic of China
iminhaji@nao.cas.cn
[2] Department of Astronomy, Kyoto University, Kitashirakawa-Oiwake-cho, Sakyo-ku, Kyoto 606-8502, Japan
[3] University of Oxford, St Edmund Hall, Oxford OX1 4AR, UK
[4] Institute for Theory and Computation, Center for Astrophysics, Harvard University & Smithsonian, 60 Garden Street, Cambridge, MA 02138, USA
[5] M.I.T., Department of Physics and Kavli Institute for Astrophysics and Space Research, 70 Vassar Street, Cambridge, MA, 02139, USA
[6] National Astronomical Observatories, Chinese Academy of Sciences, Beijing 100012, People's Republic of China
Received 2022 September 29; revised 2022 November 26; accepted 2022 November 29; published 2022 December 22

Abstract

Various white-dwarf (WD) binary scenarios have been proposed trying to understand the nature and the diversity of type Ia supernovae (SNe Ia). In this work, we study the evolution of carbon–oxygen WD—red giant (RG) binaries (including the role of magnetic confinement) as possible SN Ia progenitors (the so-called symbiotic progenitor channel). Using the MESA stellar evolution code, we calculate the time dependence of the structure of the RG star, the wind mass loss, the Roche lobe-overflow mass-transfer rate, the polar mass-accretion rate (in the case of magnetic confinement), and the orbital and angular-momentum evolution. We consider cases where the WD is nonmagnetic and cases where the magnetic field is strong enough to force accretion onto the two small polar caps of the WD. Confined accretion onto a small area allows for more efficient hydrogen burning, potentially suppressing nova outbursts. This makes it easier for the WD to grow in mass toward the Chandrasekhar-mass limit and explode as a SN Ia. With magnetic confinement, the initial parameter space of the symbiotic channel for SNe Ia is shifted toward shorter orbital periods and lower donor masses compared to the case without magnetic confinement. Searches for low-mass He WDs or relatively low-mass giants with partially stripped envelopes that survived the supernova explosion and are found in SN remnants will provide crucial insights for our understanding of the contribution of this symbiotic channel.

Unified Astronomy Thesaurus concepts: Close binary stars (254); Red giant stars (1372); White dwarf stars (1799); Magnetic fields (994); Type Ia supernovae (1728)

1. Introduction

Type Ia supernovae (SNe Ia) are known as one of the very energetic astronomical phenomena that are key for understanding the evolution of the universe; they have generally been considered the results of thermonuclear explosions of carbon–oxygen white dwarfs (CO white dwarfs, WDs; Hoyle & Fowler 1960) in close binary systems. In both observational and theoretical studies, it is still hard to arrive at a robust conclusion on the binary stellar evolution pathways that lead to SNe Ia (for recent reviews see, e.g., Maoz et al. 2014; Maeda & Terada 2016; Livio & Mazzali 2018; Jha et al. 2019; Soker 2019), and indeed many different possible routes could contribute to the SN Ia population (see, e.g., Soker 2018 for a comparison of the different evolutionary scenarios). The SN Ia progenitor scenarios can be summarized as follows: (a) the single-degenerate (SD) scenario in which the CO WD accretes matter from a nondegenerate companion star and grows in mass toward the Chandrasekhar mass (e.g., Whelan & Iben 1973; Nomoto 1982; Li & van den Heuvel 1997; Langer et al. 2000; Han & Podsiadlowski 2004; Podsiadlowski et al. 2008; Lü et al. 2009; Ruiter et al. 2009; Di Stefano & Kilic 2012; Wang & Han 2012; Nelemans et al. 2013; Ablimit et al. 2014; Claeys et al. 2014; Ablimit & Maeda 2019a, 2019b; Liu et al. 2021; Ablimit 2022a). (b) The double-degenerate (DD) scenario that contains two WDs (of which at least one is a CO WD), which will experience a merger (e.g., Iben & Tutukov 1984; Webbink 1984; Marsh et al. 1995; Fryer et al. 2010; Toonen et al. 2012; Pakmor et al. 2013; Sato et al. 2015; Ablimit et al. 2016; Perets et al. 2019). (c) The WD–WD collision (WWC) scenario where two CO WDs collide head-on at about where their freefall velocity causes nuclear ignition at the interface (e.g., Raskin et al. 2009; Kushnir et al. 2013). (d) The core-degenerate (CD) scenario where a CO WD companion merges with the CO (or possibly HeCO) core of a massive asymptotic giant branch (AGB) star during a common-envelope (CE) phase (e.g., Kashi & Soker 2011; Soker 2011; Soker 2014). (e) The core-merger-detonation (CMD) scenario, where the merger of a CO WD with the He core of a nondegenerate evolved star during a CE phase induces a double detonation inside a common envelope (Ablimit 2021).

The initial ignition of the WD that leads to its explosion can occur in two main different ways: one is the delayed core detonation of a Chandrasekhar-mass WD (e.g., Khokhlov 1991; Roepke & Niemeyer 2007; Roepke et al. 2007; Kasen et al. 2009; Hristov et al. 2018; Lach et al. 2022); the other is a helium-shell detonation near the WD surface that subsequently leads to a carbon detonation in the core of a sub-Chandrasekhar-mass WD (e.g., Woosley & Weaver 1994; Shen et al. 2021), commonly referred to as a double detonation. The direct core ignition of a WD can happen in the SD model (with the WD+main-sequence, MS, star channel, WD+red giant, RG,

channel, etc.), the DD model (with the merger of two CO WDs, etc.), and the CD model, while the double detonation occurs in some variants of the SD model (with the WD+nondegenerate helium (He) star channel), the DD model (with collisions or mergers between a CO WD and a He WD or a hybrid HeCO WD), and the CMD model. In the case of a head-on collision (the WWC scenario), the explosion is initiated by a detonation either in the shocked region or in the contact region near the WD interface (depending on the mass of the WDs; Kushnir et al. 2013). It is still hard to constrain the detailed explosion mechanism and the progenitor models, not only because of the complexities and speculative aspects of the theoretical studies, but also because of the many intrinsic variations in observed SN Ia properties.

Observationally, photometric and spectroscopic properties of SNe Ia provide promising clues for understanding SN Ia progenitor systems and the explosion physics. SN Ia light curves observed by recent telescopes such as the Kepler spacecraft (e.g., Dimitriadis et al. 2019; Shappee et al. 2019) and the Transiting Exoplanet Survey Satellite (e.g., Fausnaugh et al. 2021) have been used to search for better constraints. However, the interpretation of these observational results is still not clear enough to allow robust conclusions (e.g., Piro & Nakar 2013; Magee et al. 2018; Stritzinger et al. 2018; Polin et al. 2019). Tiwari et al. (2022) argued that observations of the late-time light curve of SN 2015F are only consistent with a sub-Chandrasekhar-mass WD progenitor, while observations of four other events (SN 2011fe, SN 2012cg, SN 2014J, SN 2013aa) are consistent with both Chandrasekhar-mass and sub-Chandrasekhar-mass progenitors. Very recently, Burke et al. (2022) presented a sample of nine SNe Ia with exemplary early-time, high-cadence, multiwavelength follow-up from the Las Cumbres Observatory and Swift and found that their observational results are overall consistent with Roche lobe (RL) overflowing, single-degenerate progenitor systems described by companion interaction models.

Höflich et al. (2021) presented and analyzed the near-infrared spectrum of the underluminous SN Ia SN 2020qxp/ASASSN-20jq, obtained with NIRES at the Keck Observatory 191 days after *B*-band maximum. They found good agreement between the observed lines and the synthetic profiles computed from 3D simulations of off-center delayed detonations in Chandrasekhar-mass WD models. Ashall et al. (2021) presented a multiwavelength photometric and spectroscopic analysis of 13 2003fg-like SNe Ia and concluded that these observations could be reproduced by the CD and/or CMD scenario(s). Nevertheless, the observed signature in the late-time nebular spectrum and light curve of SN 2006gy presented by Jerkstrand et al. (2020) supports the CMD scenario. Siebert et al. (2020) demonstrated that SN 2019yvq is one of the best examples yet supporting the conclusion that multiple progenitor channels may be necessary to reproduce the full diversity of normal SNe Ia. Various observational characteristics are presented that indicate multiple possibilities (e.g., Taubenberger 2017). In addition we note that that the properties of observed WD populations in recent sky surveys do not support many theoretical predictions in various progenitor scenarios (e.g., Rebassa-Mansergas et al. 2013; Bauer et al. 2021; Kennea et al. 2021; Kruckow et al. 2021; Rebassa-Mansergas et al. 2021; Hernandez et al. 2022; Korol et al. 2022; Lagos et al. 2022).

The detection of electromagnetic signals in the radio and X-ray bands from the interaction between circumstellar material (CSM) and SN ejecta provides crucial clues for constraining progenitor models: the SD, CD, and CMD scenarios with nondegenerate companions are more likely to produce a hydrogen-rich or helium-rich CSM. Moreover, a very recent observational study of SN 2020eyj (Kool et al. 2022) showed the helium-rich CSM interaction in SN 2020eyj, and they suggest the SD scenario with helium star donors (e.g., Ablimit 2022a) might be the progenitor of SN 2020eyj. Interestingly, the expected CSM from the CMD scenario (especially with helium donors, see Ablimit 2021 for more details) may also produce the properties of SN 2020eyj. Observations of SN 2002ic, SN 2005gj, SN 2006X, SN 2008J, PTF 11kx, SN 2015cp, and SN 2018fhw (e.g., Hamuy et al. 2003; Aldering et al. 2006; Patat et al. 2007; Dilday et al. 2012; Taddia et al. 2012; Graham et al. 2019; Kollmeier et al. 2019; Vallely et al. 2019) demonstrated the presence of a CSM, and the WD+RG channel (a variant of the SD scenario) has been suggested as a possible origin for at least some of these (i.e., SN 2005gj, SN 2006X, SN 2008J, SN 2015cp, and SN 2018fhw). Moreover, a number of observed symbiotic recurrent nova systems (i.e., RS Oph, T CrB, and V407 Cyg) have been suggested to be observational counterparts of SN Ia progenitors in the WD+RG channel (e.g., Hachisu et al. 1999; Sokoloski et al. 2006).

The evolutionary pathway of WD+RG binaries has been studied for decades (e.g., van den Heuvel et al. 1992; O'Brien et al. 2006; Lü et al. 2009; Chomiuk et al. 2012; Lundqvist et al. 2020). It has been pointed out that the relatively higher and unstable mass-transfer rate may easily lead to CE evolution, which may reduce the contribution of the WD +RG channel to SNe Ia (e.g., Yungelson & Livio 1998; Han & Podsiadlowski 2004). There are many important unsolved physical processes, and the wind mass-loss process from RG stars is one of the particularly uncertain processes in the symbiotic channel. Some previous studies have suggested that it is a spherical stellar wind (e.g., Chomiuk et al. 2012; Lundqvist et al. 2020), while other studies consider it an a spherical wind lost from the RG star in the WD binary (O'Brien et al. 2006; Lü et al. 2009). Besides, the details of RL mass transfer from an RG donor is still poorly understood (e.g., Pastetter & Ritter 1989; Chen et al. 2010), and these main physical processes need further investigation.

Magnetism may play a crucial role in the accretion and nuclear burning processes on the WD (see Mukhopadhyay & Bhattacharya 2022 for a recent review on magnetized compact stars). The magnetic-field strength of the WD, the mass-transfer rate, the masses of the donor, and the WD are the most relevant parameters for studying the effects of magnetism in WD binary evolution (e.g., Livio 1983; Ablimit & Maeda 2019a, 2019b; Gupta et al. 2020; Hogg et al. 2021; Walters et al. 2021; Ablimit 2022a). Magnetized WDs have been detected in symbiotic binaries and supersoft X-ray sources (Kahabka 1995; Sokoloski & Bildsten 1999; Osborne et al. 2001). Ablimit & Maeda (2019a) find that highly magnetized WDs, accreting H-rich material, can lead to different outcomes in detailed WD +MS binary evolution calculations for SNe Ia (see also Ablimit & Maeda 2019b), while Ablimit (2022a) demonstrated that the contribution of the WD+He star channel to SNe Ia is moderately influenced by the magnetic field of the WD. This

suggests that the role of magnetism in WD binary evolution also needs to be investigated for the WD+RG channel.

In this work, we investigate the evolution of WD+RG binaries as a potential channel for SN Ia progenitors by considering stable mass transfer via RL overflow (RLOF; i.e., avoiding CE evolution), stellar wind mass loss, and non-magnetic and magnetic WDs with the binary version of the 1D stellar evolution code MESA (Modules for Experiments in Stellar Astrophysics). The WD+RG channel for SNe Ia is also commonly referred to as the symbiotic channel. In Section 2, we provide the main description of the binary physical processes and parameters in the detailed MESA simulations in the symbiotic channel. Results and discussions are presented in Section 3, followed by the main conclusions in Section 4.

2. MESA Binary Stellar Evolution Simulations

We simulate the detailed evolution of WD+RG binaries using the star and binary packages of version 15140 of the MESA code (Paxton et al. 2011, 2015, 2019). In the first step of our calculations, we use the star package to make an RG star module based on a typical Population I composition with hydrogen mass fraction $X = 0.70$, He mass fraction $Y = 0.28$, and metallicity $Z = 0.02$. We set *initial_zfracs* = 6 and *kappa_file_prefix* = 'a09' to call the opacity tables that are built using the more recent available solar composition, and the Henyey theory of convection with *mixing_length_alpha* = 1.8 is used in the code. To generate an RG star model, we start the evolution with a pre-main-sequence model and continue the evolution until the central helium mass fraction is $\geqslant 0.98$ (at this stage it has a pure helium core and an RG radius). We construct RG star models with masses ($M_{\rm RG}$) in the range from 0.5 to 2.0 $M_{\odot}$ with mass intervals of 0.1 $M_{\odot}$ (see also Ablimit 2022a).

With the binary package of MESA, we then simulate the evolution of CO WD+RG binaries with initial orbital periods ($P_{{\rm orb},i}$) in the range of 0.5–2000 day, using the RG donor models discussed above. For the accreting WDs, treated as point masses in the code, two initial masses, 1.2 and 1.0 $M_{\odot}$, are adopted. All relevant mechanisms for angular-momentum evolution from the system (including magnetic braking, gravitational-wave radiation, and mass loss) during the binary evolution are taken into account (see Paxton et al. 2015). If matter is lost from the system, we assume that it carries the angular momentum of either the RG or the WD, whichever is appropriate. The most important physical parameters that determine the evolution of the binaries are the initial orbital periods, initial masses of the donor and the accretor, and the mass-transfer process. Because giant stars have low surface gravities and extended atmospheres, it is not so straightforward to model the RLOF mass-transfer process (see the discussions in Pastetter & Ritter 1989; Chen et al. 2010). Here, we do not consider the complications of extended atmospheres and use the general technique developed by Kolb & Ritter (1990) to compute mass transfer, which should yield acceptable results for stars at different evolutionary stages;

$$\dot{M}_{\rm RL} = -\dot{M}_0 - 2\pi F(q_2)\frac{R_{\rm RL}^3}{GM_{\rm RG}} \times \int_{P_{\rm ph}}^{P_{\rm RL}} \times \Gamma_1^{1/2}\left(\frac{2}{\Gamma_1+1}\right)^{\left(\frac{\Gamma_1+1}{2\Gamma_1-2}\right)}\left(\frac{\kappa_{\rm B}T}{m_{\rm p}\mu}\right){\rm d}P, \quad (1)$$

where $\dot{M}_{\rm RL}$ is the RLOF mass-transfer rate, Γ_1 is the first adiabatic exponent, $P_{\rm ph}$ and $P_{\rm RL}$ are the pressures at the photosphere and at the radius when the radius of the donor is equal to its RL radius, respectively. T is the temperature of the donor, $\kappa_{\rm B}$ is the Boltzmann constant, and $\mu_{\rm ph}$ is the mean molecular weight. The effective RL radius (Eggleton 1983) of the RG donor star ($R_{\rm RL}$) can be calculated as

$$R_{\rm RL} = \left(\frac{0.49q^{2/3}}{0.6q^{2/3} + \ln(1+q^{1/3})}\right)a, \quad (2)$$

where $q = M_{\rm RG}/M_{\rm WD}$ and a is the orbital separation; $\dot{M}_0$ is

$$\dot{M}_0 = \frac{2\pi}{\exp(1/2)}F(q_2)\frac{R_{\rm RL,d}^3}{GM_d}\left(\frac{\kappa_{\rm B}T_{\rm eff}}{m_{\rm p}\mu_{\rm ph}}\right)^{3/2}\rho_{\rm ph}, \quad (3)$$

where $m_{\rm p}$ is the proton mass, and $T_{\rm eff}$ is the effective temperature of the donor; $\mu_{\rm ph}$ and $\rho_{\rm ph}$ are the mean molecular weight and density at its photosphere. The fitting function $F(q_2)$ ($q_2 = M_{\rm accretor}/M_{\rm donor}$) is

$$F(q_2) = 1.23 + 0.5\log(q_2), \quad \text{for } 0.5 \lesssim q_2 \lesssim 10, \quad (4)$$

the same as in the MESA code. Other physical assumptions are the same as in the instrumental MESA papers (e.g., Paxton et al. 2015). There are different options for configuring mass loss for RG and AGB stars in MESA; we used the following wind options for the RG branch (RGB) stellar wind mass loss;

$$\begin{aligned} &\text{cool\_wind\_RGB\_scheme} = \text{'Reimers'},\\ &\text{cool\_wind\_AGB\_scheme} = \text{'Blocker'},\\ &\text{RGB\_to\_AGB\_wind\_switch} = 1\text{d} - 4,\\ &\text{Blocker\_scaling\_factor} = 0.0003\text{d}0. \end{aligned} \quad (5)$$

It is worth noting that the wind mass-loss rate before RLOF is less than $3 \times 10^{-8}\,M_{\odot}\,yr^{-1}$ most of the time (furthermore, only a small fraction of the mass lost from the spherically (isotropic) stellar wind moves toward the WD); thus the RLOF mass-transfer rate dominates for the mass accretion during the WD binary evolution. The RLOF mass-transfer rate ($\dot{M}_{\rm RL}$) plays the decisive role in determining the nature of hydrogen and helium burning on the WD and the stability of burning affects its mass retention efficiency and how the WD grows in mass. The mass growth rate of the WD is usually written as

$$\dot{M}_{\rm WD} = \eta_{\rm H}\eta_{\rm He}\dot{M}_{\rm RL}, \quad (6)$$

where we adopt the prescription of Hillman et al. (2015, 2016) for the efficiency of hydrogen burning ($\eta_{\rm H}$) and the methods of Kato & Hachisu (2004) for the mass accumulation efficiency of helium ($\eta_{\rm He}$). The different episodes of these burning efficiencies strongly affect the results of the mass-accretion phase. The adopted prescriptions here are widely used, but different models for carbon burning would somewhat affect the growth of the WD (Brooks et al. 2017).

The stream/confined accretion and related emission on a magnetized WD has to be treated differently compared to spherically symmetric accretion onto a nonmagnetic WD (e.g., Fabian et al. 1977; Livio 1983; King & Shaviv 1984; Hameury et al. 1986; King 1993; Wickramasinghe & Ferrario 2000; Wickramasinghe et al. 2014; Ferrario et al. 2015; Mukhopadhyay et al. 2017; Ablimit 2019; Ablimit 2022a). For a sufficiently

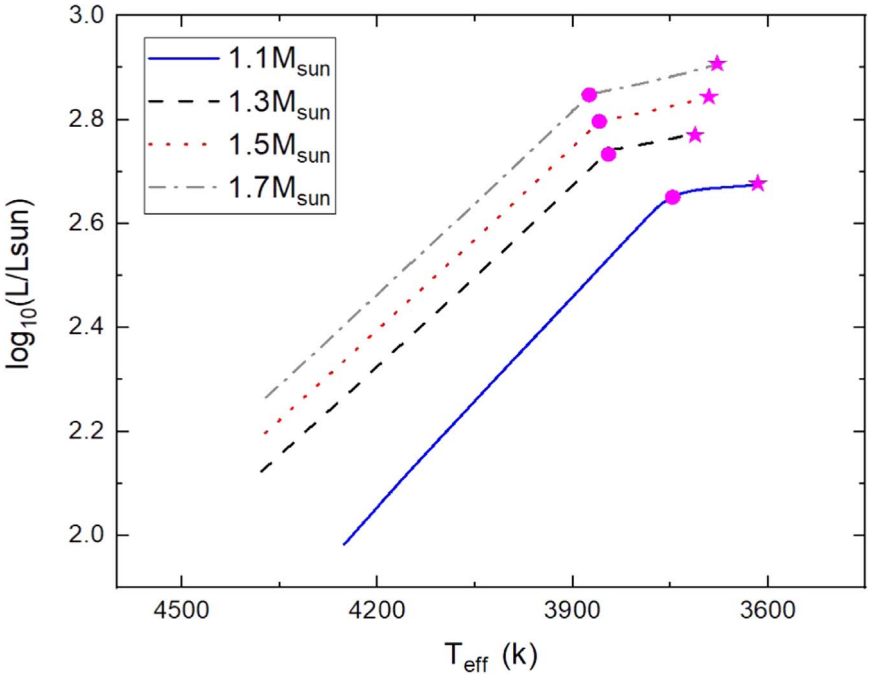

Figure 1. Hertzsprung–Russell diagram for red giant donors with different masses in nonmagnetized CO WD binaries. Red circles indicate the location where the WDs starts to accrete matter, and red stars the location when SNe Ia occur.

magnetized WD, the mass flow onto the WD, once RLOF has started, will be magnetically channeled and not through an accretion disk connected to the WD (e.g., Cropper 1990; Frank et al. 2002, see the schematic figure of Ablimit & Maeda 2019a and Ablimit 2019). The strong magnetic field of the WD controls the motion of the accreting matter near the WD; as the WD's magnetic pressure increases more rapidly than the ram pressure of the accreting material as it approaches the WD's surface, there will be a radius, the magnetospheric radius, at which the magnetic pressure is equal to the ram pressure (Frank et al. 2002). Below this radius, matter will flow along magnetic-field lines and fall onto the magnetic poles of the WD through an accretion column. The minimum physical condition for magnetically confined accretion is that the magnetic-field strength (B) satisfies (Livio 1983)

$$B \geqslant 9.3 \times 10^{7}\left(\frac{R_{\rm WD}}{5 \times 10^{8}\ {\rm cm}}\right)\left(\frac{P_{\rm b}}{5 \times 10^{19}\ {\rm dyne\ cm^{-2}}}\right)^{7/10} \times \left(\frac{M_{\rm WD}}{M_{\odot}}\right)^{-1/2}\left(\frac{\dot{M}}{10^{-10}\,M_{\odot}\ {\rm yr^{-1}}}\right)^{-1/2}\ {\rm G}, \quad (7)$$

where $\dot{M}$ is the RLOF mass-transfer rate ($\dot{M}_{\rm RL}$ in this work). The pressure at the base of the accreted matter ($P_{\rm b}$) is related to the properties of the WD, the size of the polar cap regions, and the accreted mass, and is taken as $P_{\rm b} = 5 \times 10^{19}$ dyne cm^{-2} (following Livio 1983). We also adopt the mass ($M_{\rm WD}$)—radius ($R_{\rm WD}$) relation of Nauenberg (1972) for the WD.

For WDs with no magnetic field or an intermediate-strength magnetic field, the mass-transfer rate has to be $\gtrsim 5 \times 10^{-8}\,M_{\odot}\ {\rm yr^{-1}}$ to avoid nova outbursts (e.g., Hillman et al. 2015, 2016). Once the magnetic-field strength of the WD meets the condition for magnetic confinement, nova outburst can be suppressed at a much lower mass-transfer rate. In this work, we adopt the approach of Ablimit & Maeda (2019a), Ablimit (2019), and Ablimit (2022a) for simulating the accretion phase of the WD, and consider WDs with no magnetic fields and WDs with intermediate and high magnetic-field strengths (B) and the effects of the magnetic fields on the binary evolution. We take a sufficiently magnetized WD with a fixed initial magnetic-field strength of 2.5×10^{7} G to realize magnetic confinement (see Livio 1983). For the purposes of deciding whether nova outbursts occur and to calculate the accretion efficiencies in Equation (6), we define an equivalent, isotropic polar mass-transfer rate ($\dot{M}_{\rm p}$) in the case of magnetic confinement as (see also Ablimit & Maeda 2019a)

$$\dot{M}_{\rm p} = \frac{S}{\Delta S}\dot{M}_{\rm RL}, \quad (8)$$

where the ratio of the surface area of the WD and the two polar regions of the WD (on which material is accreted) is $S/\Delta S = 2R_{\rm m}/(R_{\rm WD}\cos^{2}\theta)$, where we take $\theta = 0$ (the angle between the rotation axis and the magnetic-field axis; see Ablimit 2022a for more information) for the simulations in this work. $R_{\rm m}$ is the magnetospheric radius that is related with Alfvén radius $R_{\rm A}$ (Lamb et al. 1973; Norton & Watson 1989; Frank et al. 2002)

$$R_{\rm m} = \phi R_{\rm A} = \phi\ 2.7 \times 10^{10} M_{\rm WD}^{-1/7}\dot{M}_{\rm acc}^{-2/7}\mu^{4/7}\ {\rm cm}, \quad (9)$$

where ϕ is a parameter ($\leqslant 1$) that takes into account the departure from the spherically symmetric case, $\mu = BR_{\rm WD}^{3}$ is the magnetic moment of the WD in units of 10^{33} G cm^{3}, $\dot{M}_{\rm acc}$ is the mass-accretion rate in units of 10^{16} g s^{-1}, and $M_{\rm WD}$ is the WD mass in solar units.

3. Results and Discussion

The Hertzsprung–Russell (H-R) diagram in Figure 1 shows that the RG stars modeled with the MESA code in this work fit

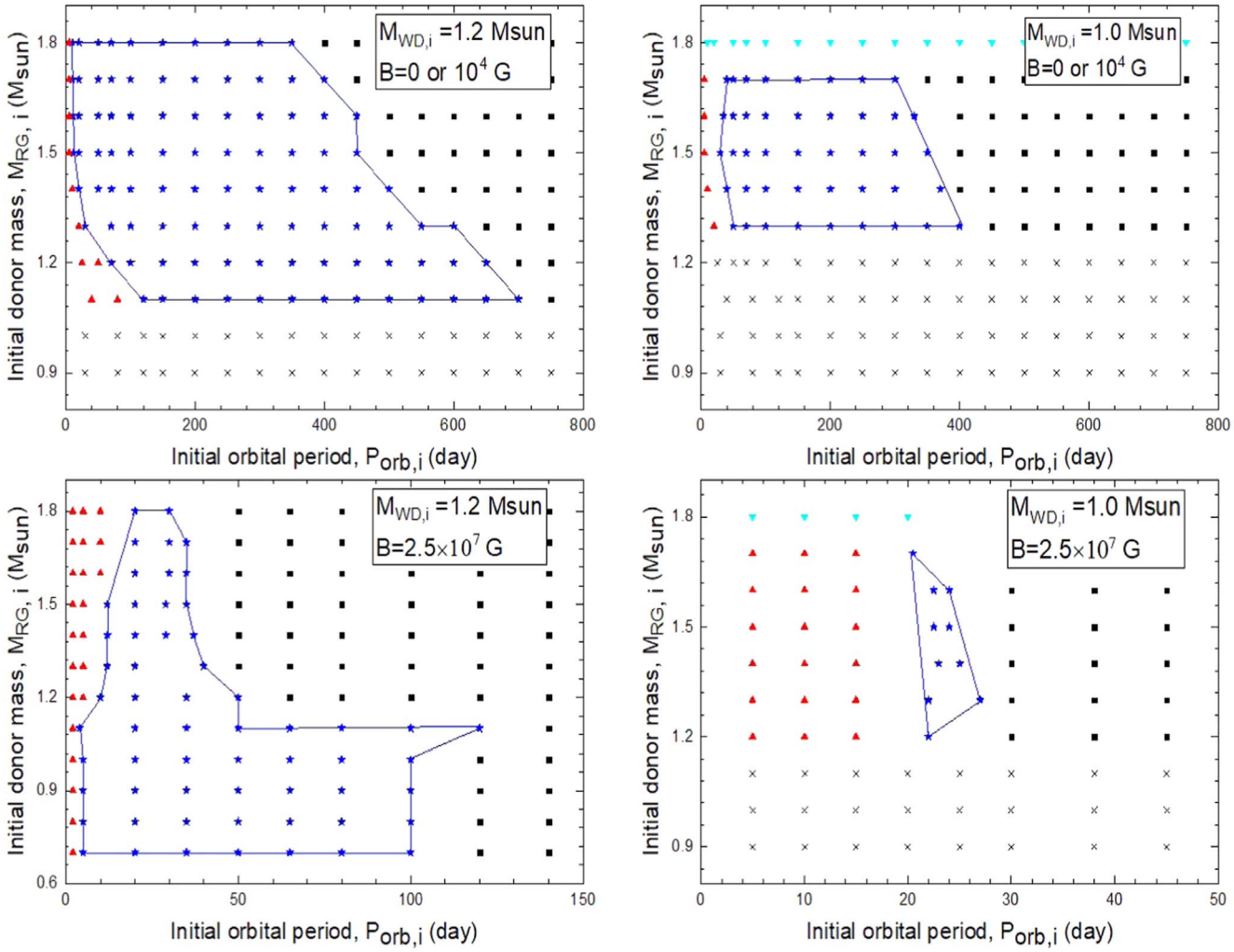

Figure 2. Initial parameter space for producing SNe Ia: the initial orbital period ($P_{\rm orb,i}$)—initial red giant donor mass ($M_{\rm RG,i}$) plane for WD+RG systems. The initial WD masses are 1.0 and 1.2 $M_\odot$. The panels show the results for WDs with no or intermediate-strength magnetic fields (upper panel), and high magnetic fields (lower panel), respectively. Blue stars show the cases that produce SNe Ia. The solid blue lines show the parameter regions within which SNe Ia are produced. The cyan triangles in the upper regions in the figure indicate the occurrence of a common envelope, and the black crosses in the lower regions show where nova outbursts occur. The red triangles and black squares on the sides show regions with inefficient mass transfer.

with our current understanding of stellar evolution (note that the figure only shows theoretical evolution tracks without observational constraints). Figure 2 shows the outcomes of the binary evolution sequences in the initial RG donor mass—initial orbital period plane, where the blue solid lines enclose the regions that produce SNe Ia (i.e., regions where the WDs grow in mass and reach the Chandrasekhar-mass limit, taken as $M_{\rm Ch} = 1.38\ M_\odot$), for different magnetic-field strengths. The upper panels of Figure 2 are for the initial parameter space of CO WD+RG star binaries with $M_{{\rm WD},i} = 1.2$ and $1.0\,M_\odot$ with no magnetic fields or intermediate magnetic-field strength, for which no magnetic confinement occurs. The ranges of initial donor mass and orbital period for the case without magnetic confinement with $M_{{\rm WD},i} = 1.2$ and $1.0\,M_\odot$ are 1.1–1.8 $M_\odot$ and 10–750 day, and 1.3–1.7 $M_\odot$ and 35−400 day, respectively. For the highly magnetized WDs with $M_{{\rm WD},i} = 1.2$ and $1.0\,M_\odot$ (with magnetic confinement; lower panels of Figure 2), they are 0.7–1.8 $M_\odot$ and 5–120 days, and 1.2–1.7 $M_\odot$ and 20–28 days, respectively. Compared to previous similar studies (e.g., Li & van den Heuvel 1997; Lü et al. 2009; Wang & Han 2010; Liu et al. 2019), the ranges from both models (those with and without magnetic confinement) are different for the following reasons: (1) The treatment of mass transfer varies for the different stellar evolution codes. Here, we use the MESA code with the Kolb scheme for the RLOF mass transfer. (2). Both wind mass loss and RLOF mass transfer are considered at the same time in our simulations. This is important as RG stars can experience substantial wind mass loss, which tends to widen the orbits prior to the beginning of RLOF. Some RG stars (near the upper mass range) can lose up to ∼32% of their mass through their stellar winds, which can increase the orbital period by ∼21% prior to RLOF. This may help to stabilize the RLOF mass transfer in some binaries. We take both wind mass loss and RLOF mass transfer into account while previous studies only considered one of them. Compared to the case without magnetic confinement, the initial donor mass can be lower for the high magnetic-field case, because magnetic confinement leads to a higher $\dot{M}_{\rm p}$, which in turn allows matter to burn more stably and increases $\dot{M}_{\rm WD}$ even in lower-mass donor stars. The ranges of initial orbital periods that produce SNe Ia shrink because the mass loss from the system is generally higher for the higher values of $\dot{M}_{\rm p}$ (the WD eject some of the transferred mass when $\dot{M}_{\rm p} > 10^{-6}\,M_\odot\ {\rm yr}^{-1}$).

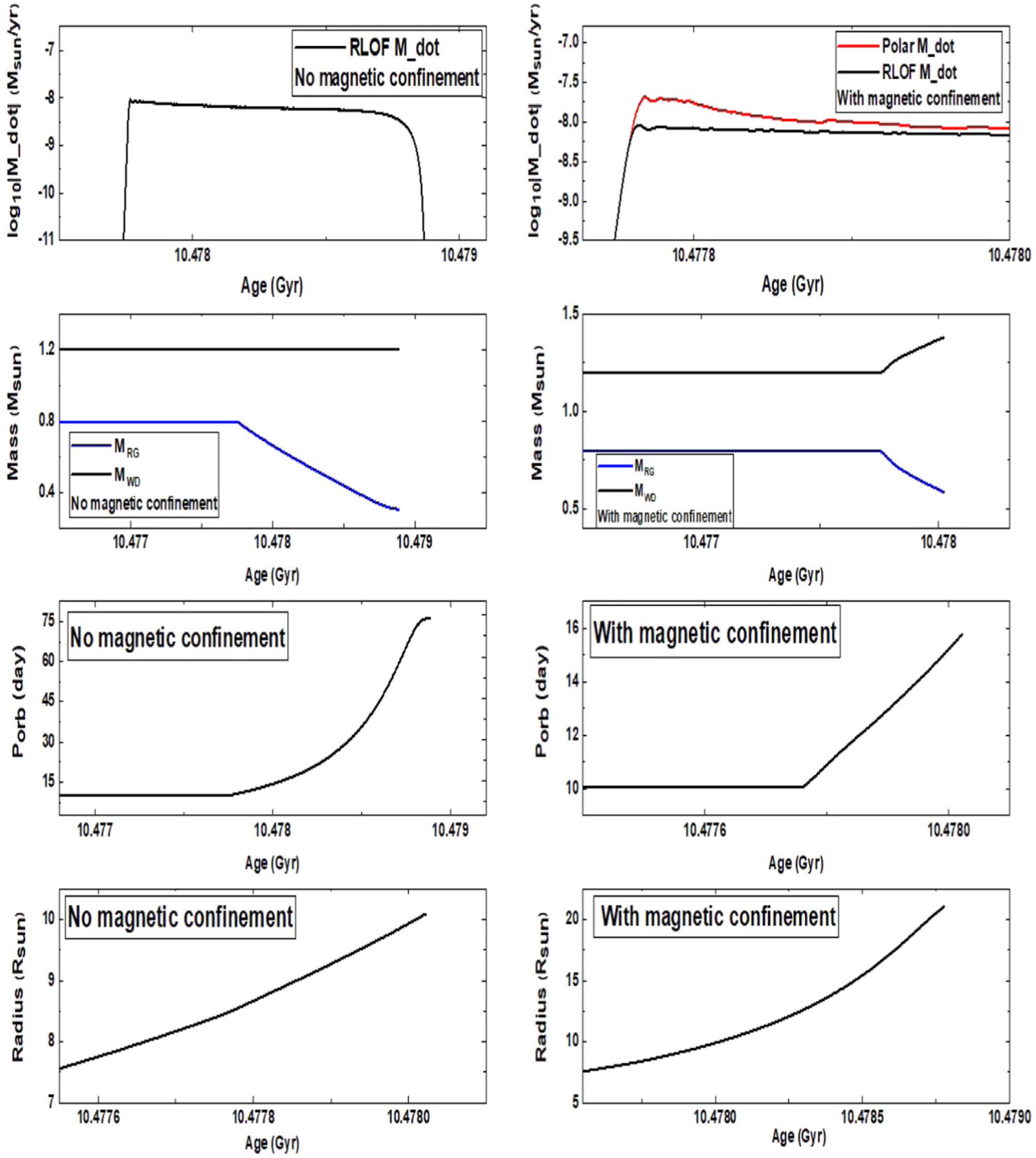

Figure 3. Detailed evolution of CO WD+RG binaries as a function of time using the MESA code. The left panels show the case of a nonmagnetic WD and the right panels the case of a magnetized WD (with $B = 2.5 \times 10^7$ G). All other initial parameters are the same: the initial masses of the WDs and donor stars are 1.2 $M_\odot$ and 0.8 $M_\odot$, respectively, with an initial orbital period of 10 days. The evolution of mass transfer, WD/donor mass, orbital period, and the radius of the donors are shown. Wind mass loss is very low ($<5 \times 10^{-13}\ M_\odot$/yr) and is not shown for clarity. RLOF M_dot and Polar M_dot in the figures are $\dot{M}_{\rm RL}$ and $\dot{M}_{\rm p}$ in the text, respectively.

Figure 3 shows the detailed binary evolution of one WD +RG system without and with magnetic confinement. Without magnetic confinement (left panels of Figure 3), the RG with an initial mass of $0.8\,M_\odot$ cannot let the WD ($M_{{\rm WD},i} = 1.2\,M_\odot$) grow in mass to the Chandrasekhar-mass limit as the low mass-transfer rate leads to nova outbursts with no significant accretion. With the effect of the WD's strong magnetic field (right panels of Figure 3), the transferred matter can be confined to the polar cap regions, and the higher polar mass-accretion rate (red line) alters the mass-accretion phase of the binary. The main difference of these two cases with the same RLOF mass transfer from the donor is that the hydrogen burning efficiency (mass retention efficiency) on the WD due to the magnetic confinement is higher than that in the spherical accretion case. As the RG star loses its mass, the WD gains mass smoothly due to the magnetic confinement, and this mass

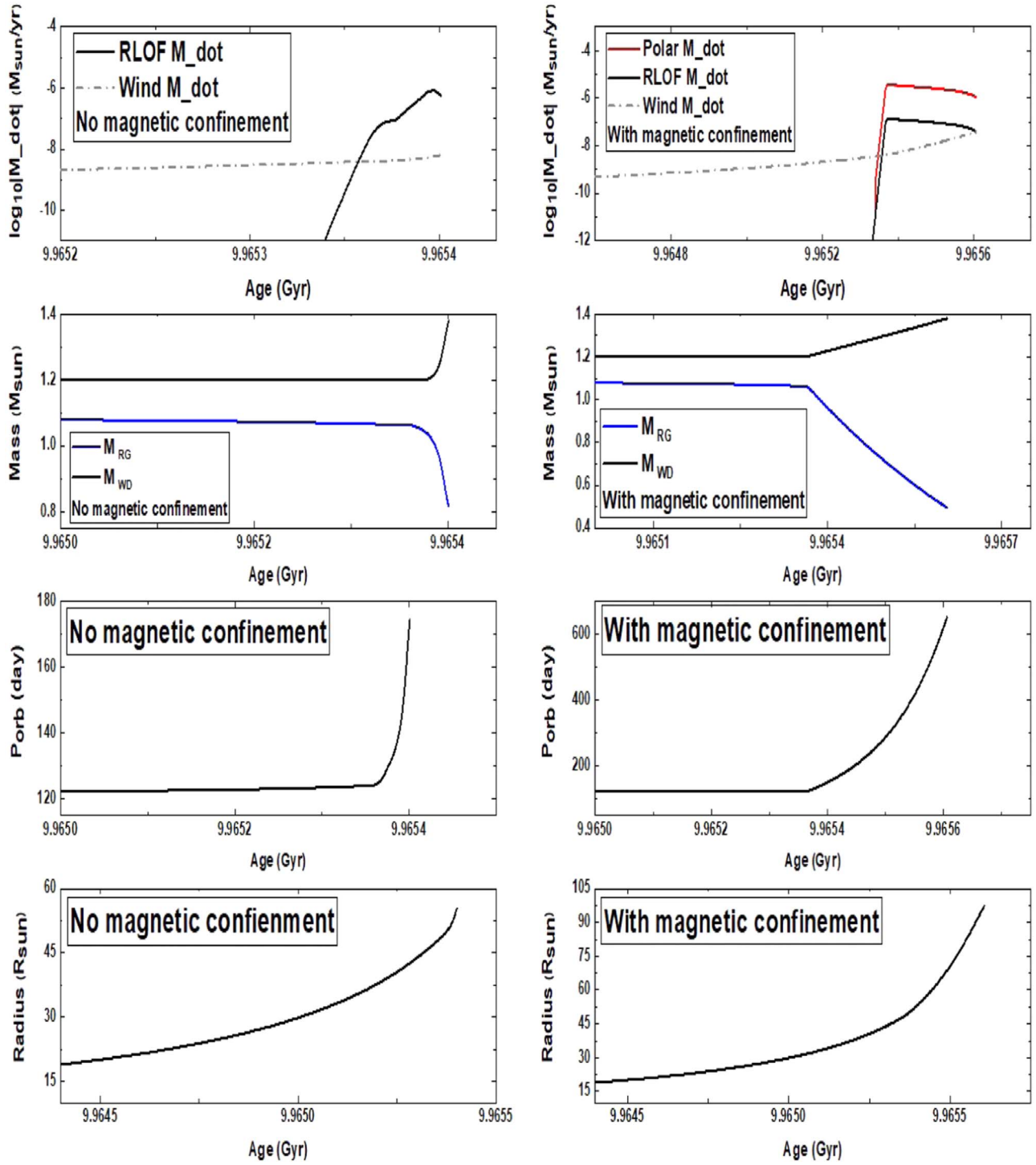

Figure 4. Another example for the detailed evolution of CO WD+RG binaries using the MESA code: evolution of mass transfer, wind mass loss, WD/donor mass, orbital period, and radius of the donors are shown as a function of time. The right and left panels are for a nonmagnetized and highly magnetized WD ($B = 2.5 \times 10^7$ G) with magnetic confinement, respectively. The initial masses of the WD and RG donors are 1.2 and 1.1 $M_{\odot}$,and the initial orbital period is 120 days for both cases.

accretion leads to a contraction of the orbit. In contrast, the WD's mass remains constant (i.e., experiences no significant accretion) without magnetic confinement, and the transferred mass will be lost from the binary, and this mass loss, including the RG stellar wind mass loss, will take angular momentum with it. Thus, the orbital period evolves from 10 to 75 days in the nonmagnetic case. In the magnetic confinement case, the orbital period evolves in a much slower way because the system loses only a small amount of mass through the RG stellar wind (the WD accretes the mass transferred through RLOF from the RG). Because of the different mass accretion, the radius of the RG star expands more than in the case of an RG without magnetic confinement.

In Figure 4, we show another example for the evolution of a WD+RG binary, where the WD ($M_{\mathrm{WD},i} = 1.2\,M_{\odot}$) can reach M_{Ch} with and without magnetic confinement, and the mass transfer in both cases proceeds on a thermal timescale. The main difference between the evolution of the two cases is that

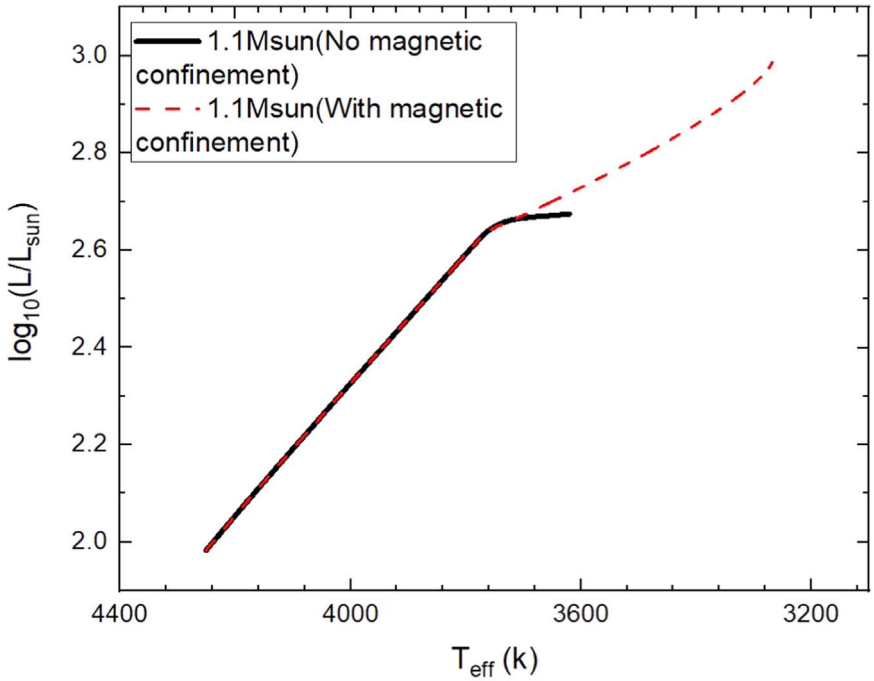

Figure 5. Example of the evolution of an RG star in the Hertzsprung–Russell diagram for the CO WD+RG binaries without and with magnetic confinement.

the accretion rate per unit area on the WD is higher with magnetic confinement. In this binary, the wind mass-loss rate of the RG star with an initial mass of 1.1 $M_\odot$ is higher than $10^{-10}\,M_\odot\,\mathrm{yr}^{-1}$ and can be as high as $10^{-8}\,M_\odot\,\mathrm{yr}^{-1}$; it takes more angular momentum away from the binary; thus, the wind mass loss widens the orbit significantly compared to the previous example. With the higher-mass donor (higher RLOF mass-transfer rate), the polar mass-transfer rate will be higher, and the outcomes will accordingly be different. In the magnetic confinement case (right panels), some of the transferred mass via RLOF would be lost from the binary and take away angular momentum; the mass loss rate will be higher if $\dot{M}_\mathrm{p}$ (red line) is higher (when it exceeds $10^{-6}\,M_\odot\,\mathrm{yr}^{-1}$), and some of the transferred matter cannot burn stably on the WD and escape from the WD. Thus, the RG donor loses more mass in order to allow the WD to grow in mass to M_Ch, and this mass loss also widens the binary orbit more compared to the case of no magnetic confinement (left panels).

There are some differences in other properties (i.e., radius, see Figure 4; luminosity and effective temperature, see Figure 5) of the giant donors in the two cases due to the different mass accretion/mass loss (or/and different initial conditions). The giant donor in the magnetic confinement case loses more mass and evolves further toward lower mass than the final donor in the case without magnetic confinement. Thus, the total ranges of orbital period and donor properties (mass, orbital velocity, luminosity, effective temperature) at the time of the SN explosion are different in the two cases. For the case without magnetic confinement, combining the results for $M_{\mathrm{WD},i} = 1.2$ and $1.0\,M_\odot$, the ranges of orbital periods, donor mass, orbital velocity, luminosity, and effective temperature are 21.3–2521.5 days, 0.59–1.23 $M_\odot$, 13.5–57.7 km s^{-1}, 1.94–3.62 (in $\log(L/L_\odot)$), and 2960−4458 K, respectively, while for the magnetic confinement case they are 5–652 days, 0.41–1.21 $M_\odot$, 22.3–100.5 km s^{-1}, 1.08–2.83 (in $\log(L/L_\odot)$), and 3268–4700 K, respectively. In both examples, the ages of the RG stars are very long, implying that the WD+RG channel has a long delay time between the star formation phase and the time of the SN explosion, and hence this channel would contribute to the old population of SNe Ia. The giant stars will survive after the SN explosion and finally evolve to become WDs. The existence of single WDs (especially low-mass He WDs with $<0.45\ M_\odot$) could be the survivors from SNe Ia produced by this channel. Indeed, a population of low-mass, apparently single WDs, presumably He WDs, has been found in the cluster NGC 6791 (Kilic et al. 2007) and in the field (Bergeron & Leggett 2002; Kawka et al. 2006) and have been proposed to be SN Ia survivors (Justham et al. 2009). Besides, some observed symbiotic novae appear to occur in binaries with very massive WDs and relatively low-mass giant companions; these systems are potential observational counterparts of SN Ia progenitors, e.g., RS Oph (e.g., Brandi et al. 2009; Mikołajewska & Shara 2017), T CrB (e.g., Belczynski & Mikołajewska 1998), and V745 Sco (e.g., Drake et al. 2016; Orlando et al. 2017). The properties of these symbiotic nova systems can be well reproduced by the WD+RG binary evolutionary sequences with and without magnetic confinement. For future observations, it will be very interesting and challenging to find the surviving He WDs or stripped giant stars whose envelopes have been partially lost by the stellar wind and/or during the mass-transfer phase in the supernova explosion, which would be less massive and hotter than comparable single stars. In addition, detailed observations of SN Ia environments can provide further clues, and the CSM properties from SNe Ia observations may constrain this model as the wind mass loss may create a CSM-like environment around the system in this symbiotic channel (but see also Moriya et al. 2013). In addition, some observational clues such as continued observations of late-time light curves of nearby SNe Ia, new high-cadence survey capacities in the short term (Ivezić et al. 2019), and future direct observations via gravitational waves (Korol et al. 2018) will provide crucial information on the nature of the SN Ia progenitors. Additionally, the evolution of oxygen-neon-magnesium composition WD—RG binaries via

accretion-induced collapse provides a promising channel to form peculiar neutron star X-ray binaries (Ablimit 2022b).

4. Conclusion

As already discussed in the Section 1, both observational and theoretical studies to date suggest that a number of progenitor models may contribute to the SN Ia population. In this study, we employed the MESA stellar evolution code to simulate a large grid of WD+RG binaries as potential SN Ia progenitors, considering WDs without magnetic field, with intermediate, and high magnetic-field strengths in these binaries. In the simulations, the RLOF mass-transfer rate is always higher than the wind mass-loss rate, and the mass-accretion phase is dominated by RLOF mass transfer, while the stellar wind causes mass loss from the systems (which mainly affects the orbital period by taking away angular momentum).

Compared to systems with WDs with no or intermediate magnetic-field strength (where magnetic confinement does not occur), highly magnetized WDs can confine the transferred matter to their polar caps and can increase the burning efficiency even with a lower mass-transfer rate. With magnetic confinement, systems with a lower-mass RG star can drive the WD to grow in mass to experience an SN explosion, as shown in the initial parameter space of the RG mass and orbital period. In the case without magnetic confinement, the initial parameter space (initial donor mass and initial orbital period) derived in this study for producing SNe Ia (for $M_{\rm WD,i} = 1.2$ and $1.0\,M_{\odot}$) are 1.1–$1.8\,M_{\odot}$ and 10–750 days, and 1.3–$1.7\,M_{\odot}$ and 35–400 days, respectively. For the highly magnetized WDs (for $M_{\rm WD,i} = 1.2$ and $1.0\,M_{\odot}$), they are 0.7–$1.8\,M_{\odot}$ and 5–120 days, and 1.2–$1.7\,M_{\odot}$ and 20–28 days, respectively. Based on the two examples for which we derived the post-SN properties, we suggest that finding a He WD or an RG with an envelope that has at least partially been stripped, lower-mass giant (and/or hotter) stars after the SN or inside an SN remnant will provide a conclusive test for this symbiotic scenario. In the future we will also consider the possibility of super-Chandrasekhar WDs and the contribution of highly magnetized WDs in binaries with MS, RG, and stripped helium star companions to the class of overluminous SNe Ia (I. Ablimit et al. 2023, in preparation).

We thank Noam Soker for useful comments and discussions. This work is supported by NSFs.

Software: Modules for Experiments in Stellar Astrophysics (MESA; Paxton et al. 2011, 2015, 2019).

Data Availability

The data underlying this article will be shared on reasonable request to the corresponding author.

ORCID iDs

Iminhaji Ablimit https://orcid.org/0000-0001-7003-4220
Philipp Podsiadlowski https://orcid.org/0000-0002-8338-9677
Saul A. Rappaport https://orcid.org/0000-0003-3182-5569

References

Ablimit, I. 2019, ApJ, 881, 72
Ablimit, I. 2021, PASP, 133, 074201
Ablimit, I. 2022a, MNRAS, 509, 6061
Ablimit, I. 2022, MNRAS, Advance Access
Ablimit, I., & Maeda, K. 2019a, ApJ, 871, 31
Ablimit, I., & Maeda, K. 2019b, ApJ, 885, 99
Ablimit, I., Maeda, K., & Li, X.-D. 2016, ApJ, 826, 53
Ablimit, I., Xu, X.-J., & Li, X.-D. 2014, ApJ, 780, 80
Aldering, G., Antilogus, P., Bailey, S., et al. 2006, ApJ, 650, 510
Ashall, C., Lu, J., Hsiao, E. Y., et al. 2021, arXiv:2106.12140
Bauer, E. B., Chandra, V., Shen, K. J., & Hermes, J. J. 2021, ApJL, 923, L34
Belczynski, K., & Mikołajewska, J. 1998, MNRAS, 296, 77
Bergeron, P., & Leggett, S. K. 2002, ApJ, 580, 1070
Brandi, E., Quiroga, C., Mikołajewska, J., Ferrer, O. E., & Garcia, L. G. 2009, A&A, 497, 815
Brooks, J., Schwab, J., Bildsten, L., Quataert, E., & Paxton, B. 2017, ApJ, 843, 151
Burke, J., Howell, A., Sand, D. J., et al. 2022, arXiv:2207.07681
Chen, X., Podsiadlowski, P., Mikołajewska, J., & Zhanwen, H. 2010, in AIP Conf. Proc. 1314 (Melville, NY: AIP), 59
Chomiuk, L., Soderberg, A. M., Moe, M., et al. 2012, ApJ, 750, 164
Claeys, J. S. W., Pols, O. R., Izzard, R. G., Vink, J., & Verbunt, F. W. M. 2014, A&A, 563, A83
Cropper, M. 1990, SSRv, 54, 195
Di Stefano, R., & Kilic, M. 2012, ApJ, 759, 56
Dilday, B., Howell, D. A., Cenko, S. B., et al. 2012, Sci, 337, 924
Dimitriadis, G., Foley, R. J., Rest, A., et al. 2019, ApJL, 870, L1
Drake, J. J., Delgado, L., Laming, J. M., et al. 2016, ApJ, 825, 95
Eggleton, P. P. 1983, A&A, 268, 368
Fabian, A. C., Pringle, J. E., Rees, M. J., & Whelan, J. A. J. 1977, MNRAS, 179, 9
Fausnaugh, M. M., Vallely, P. J., Kochanek, C. S., et al. 2021, ApJ, 908, 51
Ferrario, L., de Martino, D., & Gansicke, B. T. 2015, SSRv, 191, 111F
Frank, J., King, A., & Raine, D. J. 2002, in Accretion Power in Astrophysics, ed. J. Frank, A. King, & D. Raine (Cambridge: Cambridge Univ. Press), 398
Fryer, C. L., Ruiter, A. J., Belczynski, K., et al. 2010, ApJ, 725, 296
Graham, M. L., Harris, C. E., Nugent, P. E., et al. 2019, ApJ, 871, 62
Gupta, A., Mukhopadhyay, B., & Tout, C. A. 2020, MNRAS, 496, 894
Hachisu, I., Kato, M., & Nomoto, K. i. 1999, ApJ, 522, 487
Hameury, J.-M., King, A. R., & Lasota, J.-P. 1986, MNRAS, 218, 695
Hamuy, M., Phillips, M. M., Suntzeff, N. B., et al. 2003, Natur, 424, 651
Han, Z., & Podsiadlowski, P. 2004, MNRAS, 350, 1301
Hernandez, M. S., Schreiber, M. R., Parsons, S. G., et al. 2022, MNRAS, 517, 2867
Hillman, Y., Prialnik, D., Kovetz, A., & Shara, M. M. 2015, MNRAS, 446, 1924
Hillman, Y., Prialnik, D., Kovetz, A., & Shara, M. M. 2016, ApJ, 819, 168
Höflich, P., Ashall, C., Bose, S., et al. 2021, ApJ, 922, 186
Hoyle, F., & Fowler, W. A. 1960, ApJ, 132, 55
Hogg, M. A., Cutter, R., & Wynn, G. A. 2021, MNRAS, 500, 2986
Hristov, B., Collins, D. C., Hoeflich, P., Weatherford, C. A., & Diamond, T. R. 2018, ApJ, 858, 13
Iben, I., & Tutukov, A. V. 1984, ApJS, 54, 335
Ivezić, Ž., Kahn, S. M., Tyson, J. A., et al. 2019, ApJ, 873, 111
Jerkstrand, A., Maeda, K., & Kawabata, K. S. 2020, Sci, 367, 415
Jha, S. W., Maguire, K., & Sullivan, M. 2019, NatAs, 3, 706
Justham, S., Wolf, C., Podsiadlowski, P., & Han, Z. 2009, A&A, 493, 1081
Kahabka, P. 1995, in ASP Conf. Ser. 85, ed. D. A. H. Buckley & B. Warner (San Francisco, CA: ASP), 432
Kasen, D., Ropke, F. K., & Woosley, S. E. 2009, Natur, 460, 869
Kashi, A., & Soker, N. 2011, MNRAS, 417, 1466
Kato, M., & Hachisu, I. 2004, ApJ, 613, 129
Kawka, A., Vennes, S., Oswalt, T. D., Smith, J. A., & Silvestri, N. M. 2006, ApJL, 643, L123
Kennea, J. A., Coe, M. J., Evans, P. A., et al. 2021, MNRAS, 508, 781
Khokhlov, A. M. 1991, A&A, 245, L25
Kilic, M., Stanek, K. Z., & Pinsonneault, M. H. 2007, ApJ, 671, 761
King, A. R. 1993, MNRAS, 261, 144
King, A. R., & Shaviv, G. 1984, MNRAS, 211, 883
Kolb, U., & Ritter, H. 1990, A&A, 236, 385
Kollmeier, J. A., Chen, P., Dong, S., et al. 2019, MNRAS, 486, 3041
Kool1, E. C., Johansson, J., Sollerman, J., et al. 2022, arXiv:2210.07725
Korol, V., Belokurov, V., & Toonen, S. 2022, MNRAS, 515, 1228
Korol, V., Koop, O., & Rossi, E. M. 2018, ApJL, 866, L20
Kruckow, M. U., Neunteufel, P. G., Di Stefano, R., Gao, Y., & Kobayashi, C. 2021, ApJ, 920, 86
Kushnir, D., Katz, B., Dong, S., Livne, E., & Fernandez, R. 2013, ApJL, 778, L37
Lach, F., Callan, F. P., Bubeck, D., et al. 2022, A&A, 658, A179

Lagos, F., Schreiber, M. R., Parsons, S. G., et al. 2022, MNRAS, 512, 2625
Lamb, F. K., Pethick, C. J., & Pines, D. 1973, ApJ, 184, 271
Langer, N., Deutschmann, A., Wellstein, S., & Höflich, P. 2000, A&A, 362, 1046
Li, X. D., & van den Heuvel, E. P. J. 1997, A&A, 322, L9
Liu, D., Wang, B., Ge, H., Chen, X., & Han, Z. 2019, A&A, 622, A35
Liu, Z. W., Roepke, F. K., Zeng, Y., & Heger, A. 2021, A&A, 654, 103
Livio, M. 1983, A&A, 121, L7
Livio, M., & Mazzali, P. 2018, PhR, 736, 1
Lü, G., Zhu, C., Wang, Z., & Wang, N. 2009, MNRAS, 396, 1086
Lundqvist, P., Kundu, E., Perez-Torres, M. A., et al. 2020, ApJ, 890, 159
Maeda, K., & Terada, Y. 2016, IJMPD, 25, 1630024
Magee, M. R., Sim, S. A., Kotak, R., & Kerzendorf, W. E. 2018, A&A, 614, A115
Maoz, D., Mannucci, F., & Nelemans, G. 2014, ARA&A, 52, 107
Marsh, T. R., Dhillon, V. S., & Duck, S. R. 1995, MNRAS, 275, 828
Mikołajewska, J., & Shara, M. M. 2017, ApJ, 847, 99
Moriya, T. J., Maeda, K., Taddia, F., et al. 2013, MNRAS, 435, 1520
Mukhopadhyay, B., & Bhattacharya, M. 2022, Parti, 5, 493
Mukhopadhyay, B., Rao, A. R., & Bhatia, T. S. 2017, MNRAS, 472, 3564
Nauenberg, M. 1972, ApJ, 175, 417
Nelemans, G., Toonen, S., & Bours, M. 2013, in IAU Symp. Vol. 281, Binary Paths to Type Ia Supernovae Explosions (Cambridge: Cambridge Univ. Press), 225
Nomoto, K. 1982, ApJ, 253, 798
Norton, A. J., & Watson, M. G. 1989, MNRAS, 237, 715
O'Brien, T. J., Bode, M. F., Porcas, R. W., et al. 2006, Nat, 442, 279
Orlando, S., Drake, J. J., & Miceli, M. 2017, MNRAS, 464, 5003
Osborne, J. P., Borozdin, K. N., Trudolyubov, S. P., et al. 2001, A&A, 378, 800
Pakmor, R., Kromer, M., Taubenberger, S., & Springel, V. 2013, ApJL, 770, L8
Pastetter, L., & Ritter, H. 1989, A&A, 214, 186
Patat, F., Chandra, P., Chevalier, R., et al. 2007, Sci, 317, 924
Paxton, B., Bildsten, L., Dotter, A., et al. 2011, ApJS, 912, 3
Paxton, B., Marchant, P., Schwab, J., et al. 2015, ApJS, 220, 15
Paxton, B., Smolec, R., Schwab, J., et al. 2019, ApJS, 243, 10
Perets, H. B., Zenati, Y., Toonen, S., & Bobrick, A. 2019, arXiv:1910.07532
Piro, A. L., & Nakar, E. 2013, ApJ, 769, 67
Podsiadlowski, P., Mazzali, P., Lesaffre, P., et al. 2008, NewAR, 52, 381
Polin, A., Nugent, P., & Kasen, D. 2019, ApJ, 873, 84
Raskin, C., Timmes, F. X., Scannapieco, E., Diehl, S., & Fryer, C. 2009, MNRAS, 399, L156
Rebassa-Mansergas, A., Agurto-Gangas, C., Schreiber, M. R., Gansicke, B. T., & Koester, D. 2013, MNRAS, 433, 3398
Rebassa-Mansergas, A., Solano, E., Jimenez-Esteban, F. M., et al. 2021, MNRAS, 506, 5201
Roepke, F. K., & Niemeyer, J. C. 2007, A&A, 464, 683
Roepke, F. K., Woosley, S. E., & Hillebrandt, W. 2007, ApJ, 660, 1344
Ruiter, A. J., Belczynski, K., & Fryer, C. 2009, ApJ, 699, 2026
Sato, Y., Nakasato, N., Tanikawa, A., et al. 2015, ApJ, 807, 105
Shappee, B. J., Holoien, T.-W.-S., Drout, M. R., et al. 2019, ApJ, 870, 13
Shen, K. J., Boos, S. J., Townsley, D. M., & Kasen, D. 2021, ApJ, 922, 68
Siebert, M. R., Dimitriadis, G., Polin, A., & Foley, R. J. 2020, ApJL, 900, L27
Soker, N. 2011, arXiv:1109.4652
Soker, N. 2014, MNRAS, 444, L73
Soker, N. 2018, SCPMA, 61, 49502
Soker, N. 2019, NewAR, 87, 101535
Sokoloski, J. L., & Bildsten, L. 1999, ApJ, 517, 919
Sokoloski, J. L., Luna, G. J. M., Mukai, K., & Kenyon, S. J. 2006, Natur, 442, 276
Stritzinger, M. D., Shappee, B. J., Piro, A. L., et al. 2018, ApJL, 864, L35
Taddia, F., Stritzinger, M., Phillips, M., et al. 2012, A&A, 545, L7
Taubenberger, S. 2017, Handbook of Supernovae, Vol. 317 (Berlin: Springer)
Tiwari, V., Graur, O., Fisher, R., et al. 2022, MNRAS, 515, 3703
Toonen, S., Nelemans, G., & Portegies, Z. S. 2012, A&A, 546, 70
Vallely, P. J., Fausnaugh, M., Jha, S. W., et al. 2019, MNRAS, 487, 2372
van den Heuvel, E. P. J., Bhattacharya, D., Nomoto, K., & Rappaport, S. 1992, A&A, 262, 97
Walters, N., Farihi, J., Marsh, T. R., et al. 2021, MNRAS, 503, 3743
Wang, B., & Han, Z. 2012, NewAR, 56, 122
Wang, B., & Han, Z.-W. 2010, RAA, 10, 235
Webbink, R. F. 1984, ApJ, 277, 355
Whelan, J., & Iben, I. J. 1973, ApJ, 186, 1007
Wickramasinghe, D., Bozzo, E., Kretschmar, P., et al. 2014, in Physics at the Magnetospheric Boundary, EPJ Web of Conferences, 64 (Les Ulis: EDP sciences), 03001
Wickramasinghe, D. T., & Ferrario, L. 2000, PASP, 112, 873
Woosley, S. E., & Weaver, T. A. 1994, ApJ, 423, 371
Yungelson, L., & Livio, M. 1998, ApJ, 497, 168